Cold spray HEA coating surface microstructural characterization and Mechanical testing

(Article begins on next page)

13 May 2024

Cold spray HEA coating surface microstructural characterization and mechanical testing

Raffaella Sesana [a,*], Nazanin Sheibanian [a], Luca Corsaro [a], Sedat Özbilen [b], Rocco Lupoi [b], Francesco Artusio [c]

[a] DIMEAS, Department of Mechanical and Aerospace Eng., Polytechnic of Turin, Corso Duca degli Abruzzi 24, 10129 Turin, Italy
[b] Department of Mechanical, Manufacturing & Biomedical Engineering, Trinity College Dublin, The University of Dublin, Parsons Building, Dublin, D02, Ireland
[c] TN ITALY, Central Laboratory, Corso Torino 378, Pinerolo, 10064 Torino, Italy

ARTICLE INFO

ABSTRACT

Novel High Entropy Alloy (HEA) coatings in the Al0.1-0.5CoCrCuFeNi and MnCoCrCuFeNi multi-materials systems on Mg substrate were prepared from mechanical alloyed HEA powder feedstocks and by three different Cold Spray (CS) process gas (N2) temperatures (650, 750 and 850 °C). Macro and microstructural characterization of mechanically alloyed and cold sprayed HEA coatings were carried out by macro photography, OM, SEM + EDS study, micro-hardness testing, roughness, and porosity measurements.

Mechanical alloying (MA) caused plastic deformation and fracture in harder particles. Relatively soft and ductile A1 phase and Cu-rich region particles were coarser and globular in shape. Some separate Cu-rich regions were also observed apart from A1 particles. Mn-HEA powder showed a different trend with finer particle sizes due to the more brittle nature of the powder and acicular shape. During MA, a loose structure with lots of gaps, cracks, plastic deformation signs, and small particles adhering to the particle surface is generated.

Based on the experimental data obtained, it cannot be concluded that the chemical composition of the high entropy alloy influences the roughness of the coating. The deposited volume increases with temperature only for $Al_{0.1}$ and Mg-based HEA, while for the other Al-based HEA no noticeable influences can be observed. The micro-hardness of a coating depends significantly on its chemical composition: as the percentage of aluminum increases in the samples micro-hardness increases. The hardness of the coating is significantly higher than that of the substrate, and the hardness measured at the interface is intermediate between the two values.

1. Introduction

Metallurgical science has enabled the development of alloys, which show better and tailored properties than single metals. However, traditional alloys are based on a single main element, which limits the degrees of freedom in designing an alloy composition. J. W. Yeh and B. Cantor proposed a new alloy concept, "HEA" (High Entropy Alloy), which contains at least five major elements with an atomic percentage of 5–35% [1]. Any secondary alloying elements, therefore, are characterized by an atomic percentage of less than 5% [1–10]. Current knowledge mainly focuses on the system of alloys made up of Al, Co, Cr, Cu, Fe, and Ni and those derived from it, obtained by adding other elements or substituting some of them; many other alloys are still to be explored [2]. HEAs have high potential in a wide range of applications as structural and functional materials. Empirical results have shown that high mixing entropy promotes the formation of solid solutions with simple microstructures [2]. The crystal lattice is characterized by high strains and stresses, increasing strength and hardness, and a lower sensitivity to temperature variations [1,2,9,10]. Thanks to the characteristic chemical composition consisting of multiple main elements, HEAs can present excellent properties, in many cases better than conventional alloys: high strength and hardness, considerable resistance to wear, exceptional resistance in conditions of high temperature, good structural stability and excellent resistance to corrosion and oxidation. They are of great interest for applications in many industrial fields, particularly in areas where the material is subjected to harsh conditions. The manufacture of HEAs does not require special production techniques and plants, so they can be implemented with current technologies and existing plants. The presence of multiple main elements within HEAs involves "core effects" that determine the microstructural characteristics and exceptional

Table 1
Nominal composition of HEA powders.

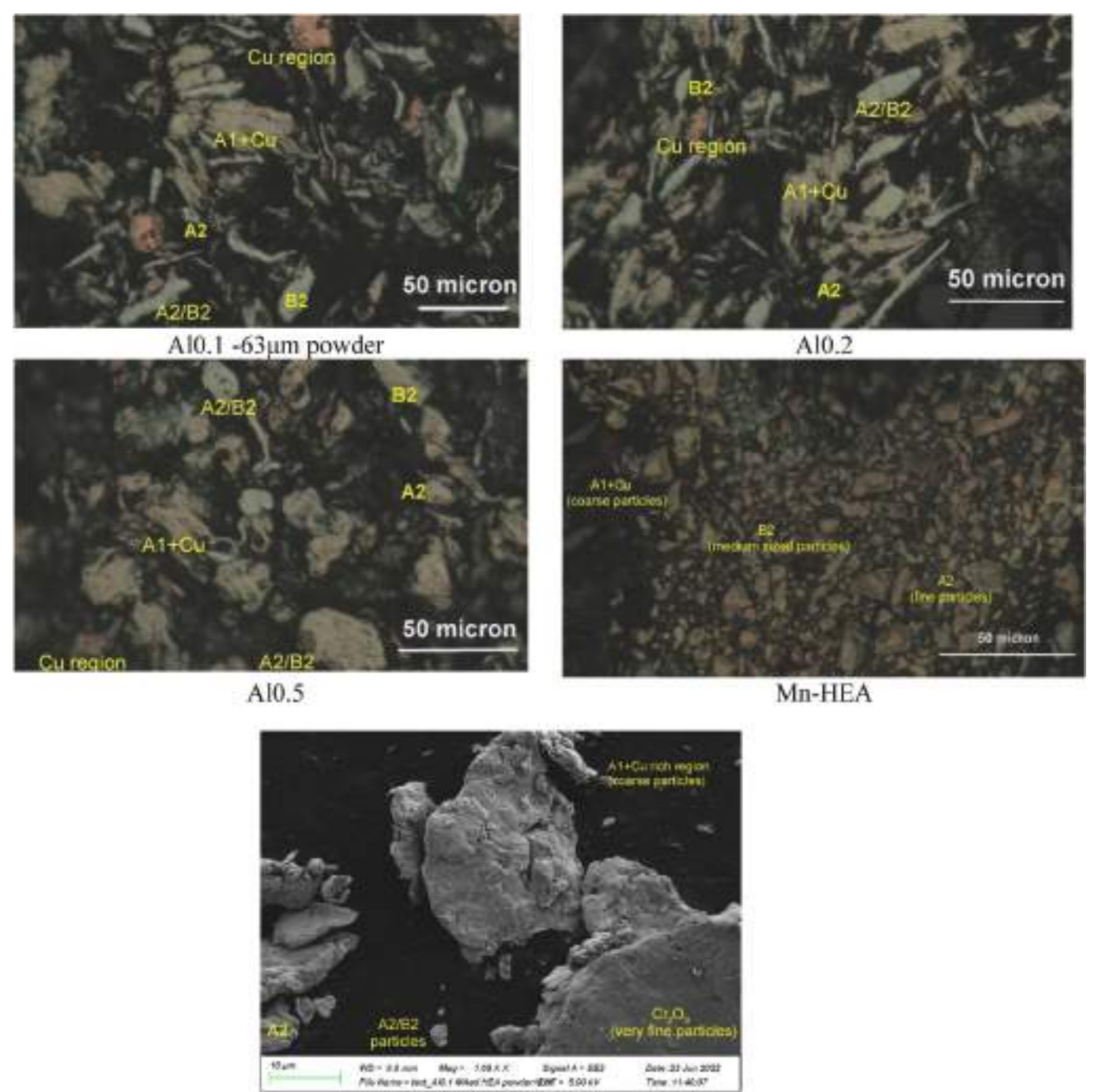| Samples Designation	Nominal chemical composition						
		Al	Cu	Cr	Co	Fe	Ni
Al$_{0.1}$CoCrCuFeNi	At%	4.22	17.38	21.2	18.67	19.74	18.79
	Wt%	1.96	19.61	19.61	19.61	19.61	19.61
Al$_{0.2}$CoCrCuFeNi	At%	8.13	16.65	20.33	17.91	18.95	18.02
	Wt%	3.85	19.23	19.23	19.23	19.23	19.23
Al$_{0.5}$CoCrCuFeNi	At%	18.3	14.8	18.09	15.96	16.84	16.0
	Wt%	9.15	18.1	18.1	18.1	18.1	18.1
MnCoCrCuFeNi	At%	–	15.62	16.81	13.6	13.6	16.86
	Wt%	–	16.7	16.7	16.7	16.7	16.7

Fig. 1. Light microscopy (LM) and powder particle surface SEM imaging (SE) of mechanically alloyed Al$_{0.1-0.5}$ (Mn)-HEA (−63 μm size fraction) feedstock powder.
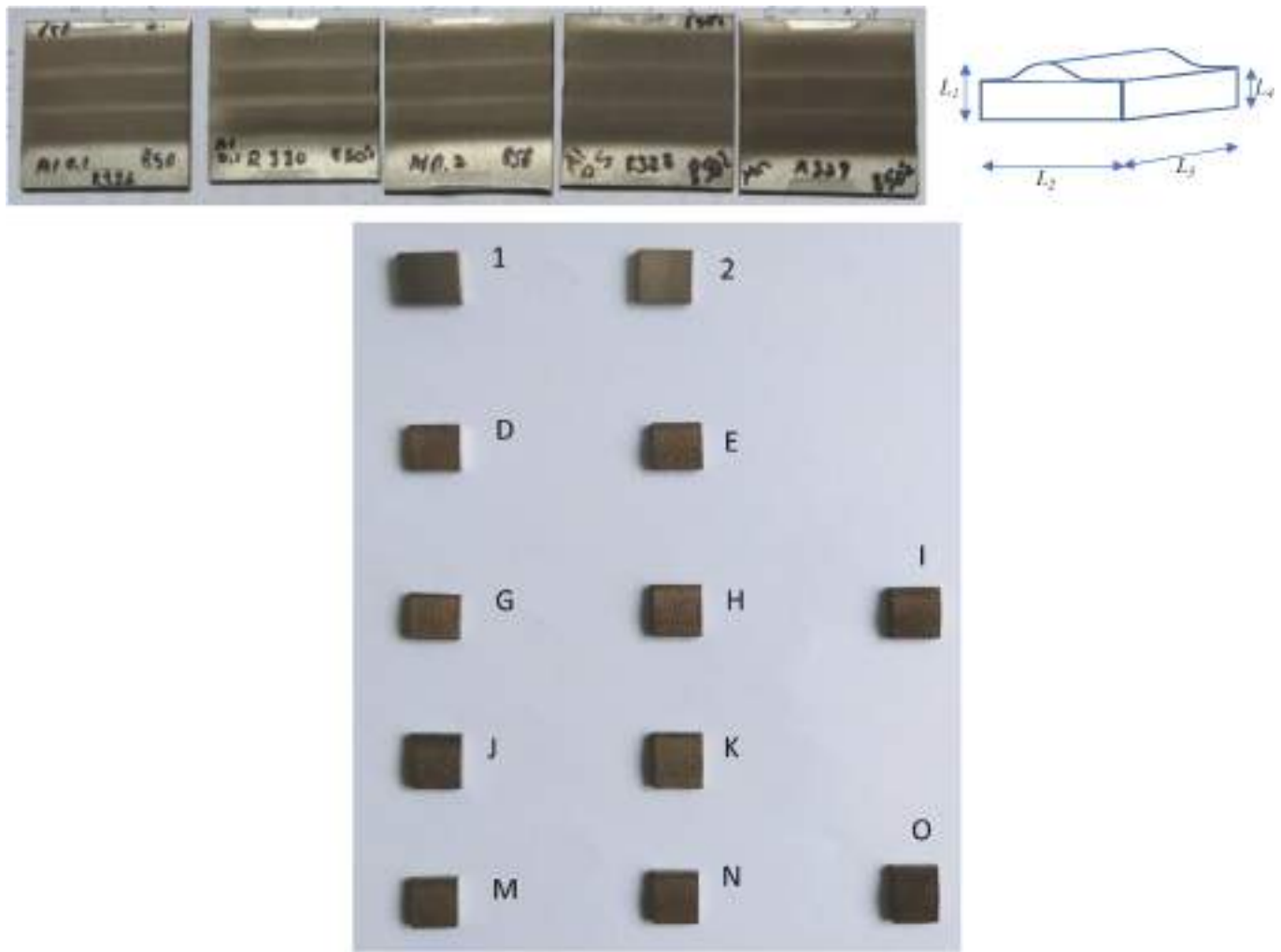
Fig. 2. Specimen nomenclature.

properties. These effects include high mixing entropy, severe distortion of the crystal lattice, sluggish diffusion, and cocktail effect [1,2,5,6,9, 10]. The first study in this regard was published [11] and considers samples of $Al_{0.5}CoCrCuFeNi$ composition quenched in water and cold rolled showed better performance than many conventional alloys, with fatigue strength limit values in the range of 540–945 MPa. These results demonstrate that the HEA of this system could be useful in future applications where fatigue strength is important. The tribological properties of HEAs are dependent on their chemical composition. The addition of elements such as Al, Fe, and Nb refines the grains and promotes the formation of phases with a BCC structure [5]. Mn and Cr also favor the formation of phases of greater hardness. As concentrations of C, N, B, and Si increase, the tribological properties improve due to the formation of carbides, silicates, and boron compounds, or the phase transformation from FCC to BCC/B2. Mo increases the hardness better than those of AISI 304 stainless steel with the same heat treatment. The wear resistance of HEAs depends on the type of phase prevailing within them. Alloys composed exclusively of simple and disordered phases ("SDPs") generally do not exhibit greater wear resistance than conventional alloys of similar hardness. However, if the prevailing phase is of the complex and ordered type ("COPs"), the wear resistance is often much higher than that of conventional alloys of similar hardness [2,12]. For this reason, one of the major applications for HEAs is represented by the creation of coatings with high wear resistance, which can be deposited using different technologies on a substrate. Composite-type coatings, in which particles of various ceramic materials are dispersed in the metal matrix, can cause an increase in the overall hardness of the coating and, consequently, a decrease in its wear rate [1,3,6–8,12–18]

This paper aims is to report on the characterization of HEA coatings obtained by cold spray, in particular dimensional and profile measurements, surface and microstructural characterization and mechanical properties (HV) determination of Cold Spray (CS) HEA coatings on Mg substrate. Two HEA compositions are investigated, one based on Al_x CoCrCuFeNi and the other on MnCoCrCuFeNi; and 3 deposition temperatures are explored: 650°, 750° and 850 °C.

2. Materials and method

Detailed characterization was performed on coating material composition, surface profile, microstructure, and interlayer.

2.1. Specimen preparation

2.1.1. Materials and mechanical alloying

Elemental powders of Al, (Mn), Co, Cr, Cu, Fe, and Ni, with high purities (>99.9%), were processed by mechanical alloying (MA) for octanary HEA mixtures: $Al_{0.1-0.5}CoCrCuFeNi$ and MnCoCrCuFeNi (all expressed in molar ratio). Details of the mechanical mixing (MM) and mechanical alloying (MA) stages are mentioned in detail in Ref. [21]. Charge calculations of pure elemental powders of Al, Cu, Co, Cr, Fe, and Ni were made to reach $Al_{0.1-0.5}CoCrCuFeNi$ and MnCoCrCuFeNi nominal composition (Table 1), accordingly. Mixing, homogenizing, and MA

Table 2

Properties of the MA $Al_{0.1-0.5}$ and Mn -HEA powder feedstocks.

HEA powder	d_{50}^a [μm]	d_m^b [μm]	Distribution mode	Particle shapes	Particle surface condition
$Al_{0.1}$	29.5	34.0	tri-modal	globular/ irregular	rough
$Al_{0.2}$	26.2	31.7	tri-modal	globular/ irregular	rough
$Al_{0.5}$	28.0	33.0	tri-modal	globular/ irregular	rough
Mn-HEA	24.2	31.1	qua-modal	globular/ irregular	rough

[a]Median particle diameter.
[b]Mean particle diameter.

Table 3

Cold spray process and denomination of chemical composition samples Al_x CoCrCuFeNi and MnCoCrCuFeNi.

$Al_{0.1}$CoCrCuFeNi	Cold spray-Temperature [°C]	650	750	–
	Denomination	D	E	
$Al_{0.2}$CoCrCuFeNi	Cold spray-Temperature [°C]	650	750	850
	Denomination	G	H	I
$Al_{0.5}$CoCrCuFeNi	Cold spray-Temperature [°C]	650	750	–
	Denomination	J	K	
MnCoCrCuFeNi	Cold spray-Temperature [°C]	650	750	850
	Denomination	M	N	O

Table 4

Specimen dimensions and weights.

Specimen Id	L_3 [mm]	L_2 [mm]	Weight [g]
D	10.09	9.39	0.4189
E	10.01	9.43	0.5829
G	10.11	9.42	0.4865
H	10.73	10.01	0.5656
I	10.72	10.01	0.5836
J	11.27	10.01	0.5622
K	11.19	9.97	0.5649
M	10.09	9.17	0.4282
N	10.59	9.21	0.5142
O	11.73	9.23	0.5807

Table 5

RTP80 roughness tester technical specifications.

Characteristic	Description/value
Measuring range [μm]	±500
Resolution [μm]	0.001
Cut-off length [mm]	0.25
Measuring length [mm]	1.5

is reported.

Specimen dimensions and weights were measured with a caliper and Mettler precision balance and reported in Table 4, according to dimensions as reported in Fig. 2.

2.2. Microstructure characterization

Details of metallographic sample preparations and microstructural characterizations were given in Ref. [24].

To assess the coating microstructure, cross-sectional samples were prepared according to standard metallographic procedures utilizing 0.06 mm colloidal silica for the final polishing. HEA powders and coating elements were analyzed using an energy-dispersive X-ray spectroscopy (EDS) unit equipped with a scanning electron microscope (SEM). During the study, coating thicknesses were measured using a Leica microscope as well as surface images were acquired using a Keyence digital microscope with a magnification of $100\times$. To evaluate the porosity of the HEA coating, binary images were analyzed using SEM.

2.3. Surface characterization measurement

An RTP80 roughness tester by SM-Instruments, was used to measure roughness. Table 5 provides a summary of the measurement specifications. The surface roughness measurements were obtained over all the specimen coatings and the two substrates. The roughness profiles were measured in directions parallel and perpendicular to the deposition direction. 0.25 mm cut-off and 1.5 mm measuring length were selected.

Three roughness measurements were made for each direction and each coating sample. Different roughness parameters were acquired. In particular: *Ra, Rq, Rt, Rz, Rp* and *Rv*. According to Standards definitions (UNI EN ISO 4287 (2011)) they are all parameters related to the amplitude of roughness, i.e. the distances between peaks and valleys. *Ra* is the arithmetical mean deviation of the assessed profile; *Rq* is the root mean square of the mean deviation of the assessed profile and it is an average amplitude measurement in the height direction; *Rt* is the maximum height of the profile, that is the distance between the maximum peak and the minimum valley, and it is related to the total height of the profile; *Rz* is the average distance between the highest peak and lowest valley in each sampling length and it is related to the maximum height of the profile; *Rp* and *Rv* the maximum peak height and valley depth over the sampling length respectively.

The surface profiles and the volume of the coating deposited on the substrate were determined for each sample, using the optical

(5.5 h) procedures were successfully applied to charge materials. MA powders were kept in plastic-sealed containers filled with Ar gas until Cold Spray (CS) processing to prevent any contamination risk from the atmosphere. A detailed description of the effect of MA on powders is reported in Ref. [24].

2.1.2. Cold spraying

Novel HEA coatings in the $Al_{0.1-0.5}$CoCrCuFeNi and MnCoCrCuFeNi multi-materials system on Mg substrate were prepared from these powder feedstocks and by cold spraying coating deposition using different Cold Spray (CS) nitrogen gas temperatures, 650,750 and 850 °C respectively (Figs. 1 and 2). The Cold Spray deposition system, available at Trinity College, Dublin, Ireland, and described in Refs. [22, 23] was used. By using variable and controlled cold spray process and coating parameters, variations in the microstructure and properties for both MA and CS $Al_{0.5}$HEA coatings were attained. CS was carried out with N_2 gas with 30 bar pressure. The nozzle used was Nz1 type, standoff distance was 47 mm, powder feed rate was 9%, nozzle speed was 15 mm s^{-1}, beam distance was 2 mm, each coating contained 4 layers, Mg substrate plate size was 50 mmx50mm, −63 μm size fraction of MA $Al_{0.5}$HEA powder feedstocks were used for CS. The nominal composition of the MA $Al_{0.1-0.5}$CoCrCuFeNi and MnCoCrCuFeNi HEA coatings [24] correspond to powder feedstock composition, reported in Table 1.

Powder properties are reported in Table 2. 10 samples of high entropy alloy (HEA) coatings, deposited on a magnesium substrate through the innovative Cold Spray (CS) deposition process, were prepared. 4 feedstock powders were used: $Al_{0.1}$CoCrCuFeNi, $Al_{0.2}$CoCrCuFeNi, $Al_{0.5}$CoCrCuFeNi and MnCoCrCuFeNi. Table 1 shows the nominal compositions of the coatings in atomic (At%) and weight (Wt%) percentages for each element present. In Ref. [24] a detailed description of the HEA coating process is described.

To distinguish the various samples, the denominations indicated in Table 3 were assigned.

Furthermore, two samples of magnesium substrates, without coating, named 1 and 2, were studied. In Fig. 2, it can be observed that the coating thickness is not uniform as it is obtained by a single pass of cold spray nozzle along a direction parallel to an edge of the specimen. In the same Fig. 2, a schematic representation of the resulting specimens
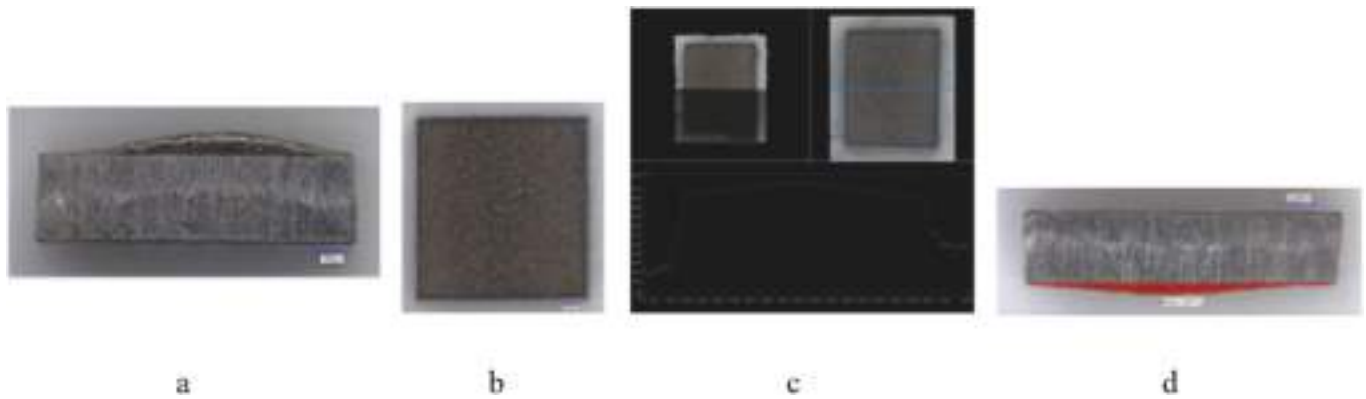
Fig. 3. Surface characterization: (a–b) the superior and the lateral surface images with a magnification of 100× respectively, (c) The average profile of the sample, (d) The Lateral surface area measurement.

profilometer functions of the Keyence VHX 7000 digital microscope. In particular, a three-dimensional scan of the upper surface of each sample was acquired, using the 3D Stitching software function. This function acquires numerous two-dimensional images and three-dimensional scans of adjacent surface portions and stitches them together to form the overall scan. Every single portion of the surface was scanned with a magnification of 100×. On the three-dimensional scan, for each sample, the profiles calculated on 60 lines parallel to each other and perpendicular to the axis of the central swelling (150 μm apart) were considered. The vector containing the mean profile data was imported into Matlab and processed. Subsequently, the area under the mean profile was calculated, which represents the area of the mean perpendicular section of the cladding. Finally, the volume of the coating was calculated by multiplying this area by the depth of the sample in the direction parallel to the axis of the bulge.

Fig. 3(a–b) illustrates the superior and lateral surface images with a magnification of 100×. The extracted average profile of the sample is shown in Fig. 3(c), while the lateral surface area measurement is shown in Fig. 3(d). The area estimation was cross-checked by measuring a polygon approximating the coating lateral area to check the order of magnitude of the computed cross-sectional area under the average profile of each specimen.

2.4. Microhardness measurement

The Innovatest Vickers microdurometer was used to measure the HV30 microhardness profiles of the coating samples with 3 N preload and 15 s of indentation time. For each specimen, the microhardness was calculated by averaging the results of 9 indentations on the polished side cross-section.

3. Result and discussion

3.1. Microstructure characterization

In Fig. 1 LM cross-sectional microstructure (−63 μm size fraction) of the $Al_{0.1-0.5}CoCrCuFeNi$ and $MnCoCrCuFeNi$ HEA powder after 5.5 h milling time is reported. Relatively fine A2 and B2 harder particles were whitish and their shape was flaky and elongated due to plastic deformation and fracture during MA. Relatively soft and ductile A1 phase and Cu-rich region particles were coarser and globular in shape. Cu-rich regions appeared as brownish-orange color and the A1 phase appeared as white with black dots due to exposure to heavy plastic deformation during MA. Some separate Cu-rich regions were also observed apart from A1 particles. This general trend of particle characteristics in Al-HEA powders was different in Mn-HEA powder where finer particle sizes due to the more brittle nature of the powder and the acicular shape of the particles were observed [24].

In the same Fig. 1, the SEM surface morphology of the $Al_{0.1}Co$-CuCrFeNi powder milled for 5.5 h shows fine to moderate size A2/B2 particles. Moreover, coarser particles for both A1 and Cu-reach regions and very fine surface Cr_2O_3 particles were observed with light microscopy (LM) and powder size distribution (PSD) study (as illustrated in Ref. [25]). It was also observed that, during mechanical alloying (5.5 h), there was a loose structure with lots of gaps, cracks, plastic deformation signs, and small particles adhering to the particle surface. Particle surfaces were also rough due to heavy plastic deformation, cold welding, and fracture mechanisms induced by MA processing. It is known that in the $Al_{0.1}CoCuCrFeNi$ HEA system, metallic elements exhibit high plasticity and go through plastic deformation, cold welding, and fracture processes, and the elemental powder size chosen during MA was influenced by their hardness and ductility.

SEM images (left column) at the interface between the as-deposited coatings and substrate are reported in Fig. 4(a–d). All the coatings showed good bonding with their substrates, free of pores and cracks. Mechanical interlocking was also observed along the coating-substrate interface. Moreover, some particles penetrated the substrate and were tightly bound by the material. Mechanical interlocking occurs as a result of the plastic deformation of the soft substrate material upon impact with the hard coating particles. Cold-sprayed coatings typically exhibit mechanical interlocking, which contributes to the coating's high adhesion strength. The cross-sectional SEM images of the coatings as deposited are shown in Fig. 4(e–h). The coatings show a dense microstructure with only a few pores, as indicated by the yellow arrows and the interparticle boundaries marked by the red arrows. Fig. 5(a) shows the quantitative analysis of the chemical elements of the coating of sample D and the mapping of the chemical elements is depicted in Fig. 5 (b). In Fig. 6 an example of image processing for porosity evaluation of specimen I is reported. Porosity results of specimens were in the range of 1.5–3.2 %.

3.2. 3.2. Surface characterization

3.2.1. Roughness measurements

The average and standard deviation (Std Dev) on 6 measurements for each sample, for the various roughness parameters, are reported in Tables 6 and 7.

Fig. 7 compares the roughness values obtained for samples with the same chemical composition at different deposition temperatures. Specimens in $Al_{0.1}CoCrCuFeNi$ show a decrease in all roughness parameters with increasing deposition temperature. For other specimens, due to the experimental scattering, a monotonic relationship between the roughness parameters and the temperature of the deposition process cannot be stated. An ANOVA analysis was performed to investigate the influence of deposition temperature and chemical composition on the *Ra* roughness parameter.
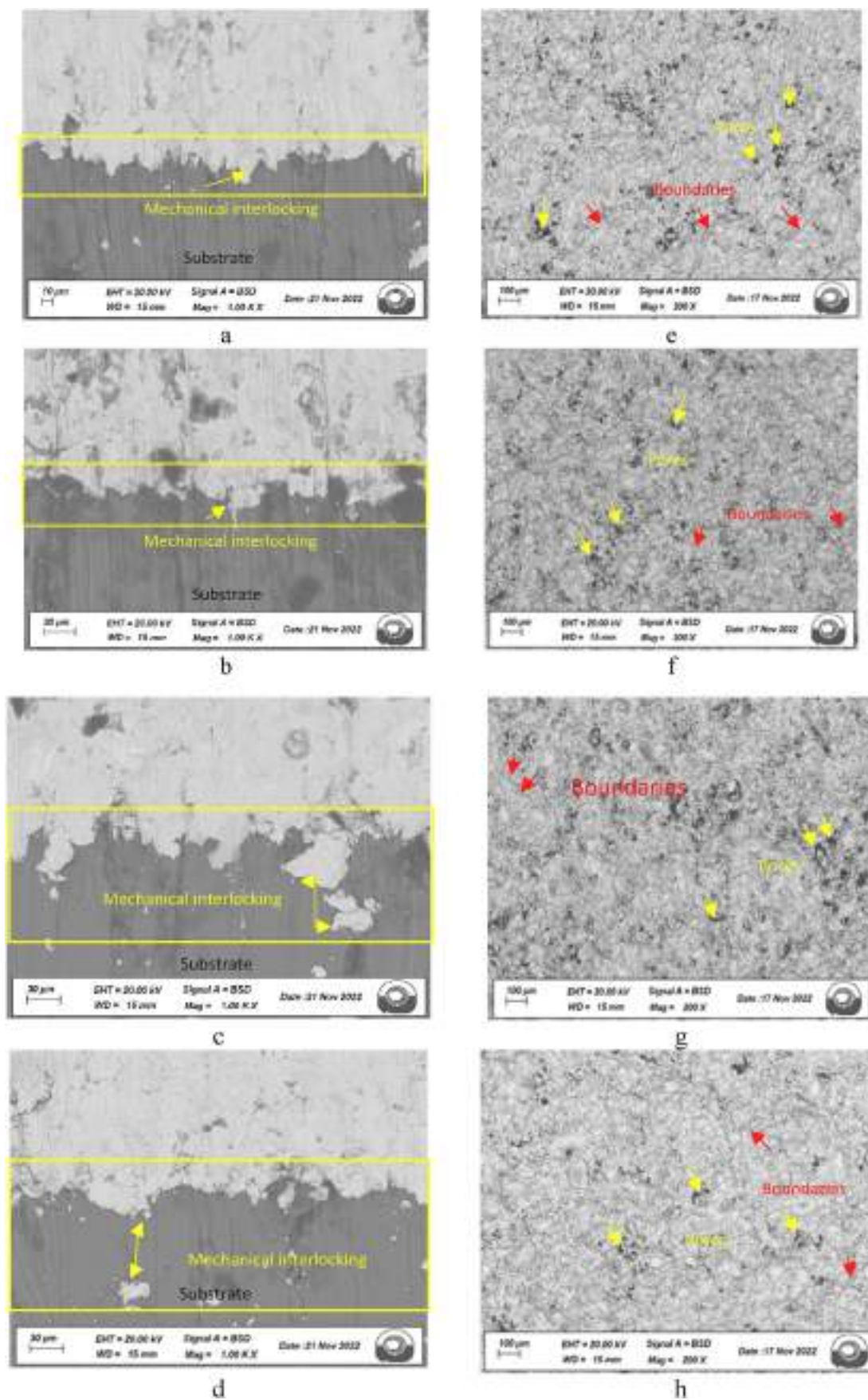
Fig. 4. Coating-substrate interfaces and coatings in cross-sectional SEM images: (a–d) Al_x CoCrCuFeNi coating, (e–f) MnCoCrCuFeNi.
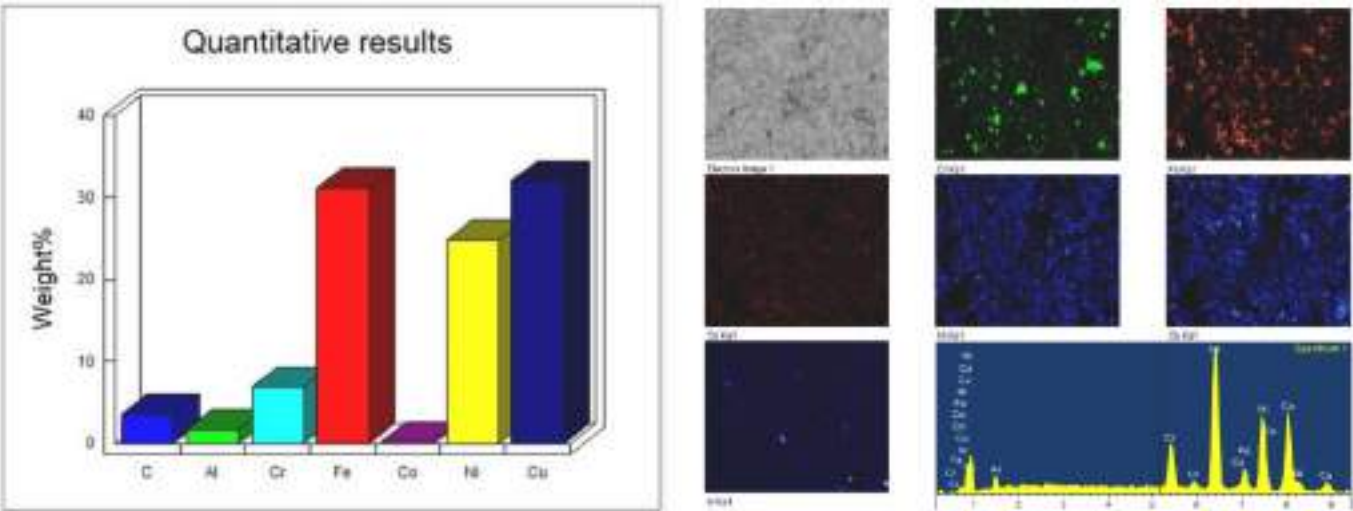
Fig. 5. SEM analysis: (a) Quantitative analysis of chemical elements of sample with composition of $Al_{0.1}$ CoCrCuFeNi, (b) EDX mapping of chemical elements of sample D.
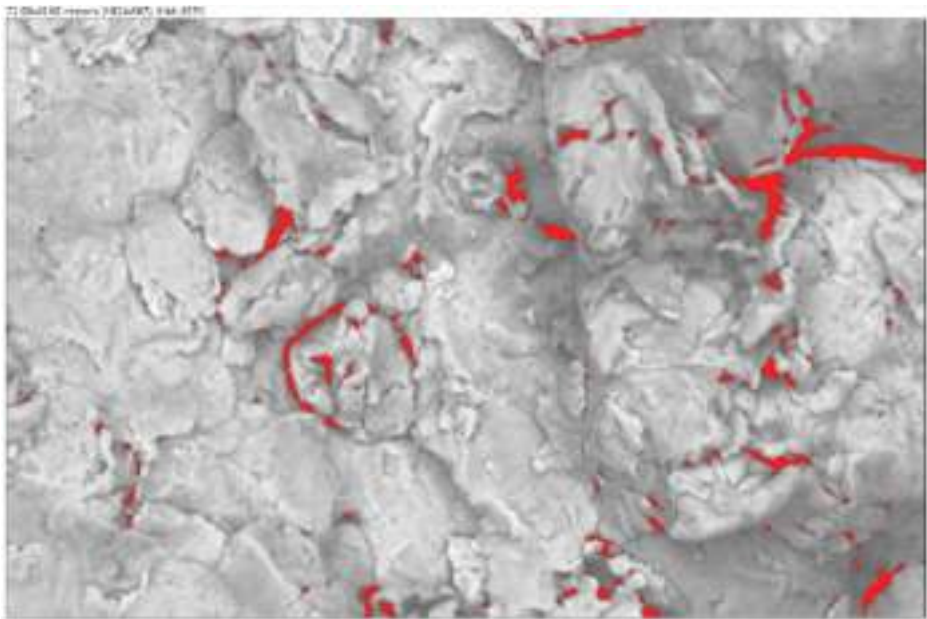

Fig. 6. Porosity analysis: SEM BSD binary image of sample I with $5000\times$ magnification.

Table 6
Average values of roughness parameters Ra, Rq, and Rt, for all samples.

Sample	*Ra*		*Rq*		*Rt*	
	Average [μm]	Std dev [μm]	Average [μm]	Std dev [μm]	Average [μm]	Std dev [μm]
D	5.912	0.461	7.217	0.560	42.757	2.318
E	4.847	0.432	5.868	0.475	31.201	3.296
G	5.006	0.850	6.083	0.875	31.669	3.826
H	5.860	0.852	7.133	1.064	38.346	9.246
I	5.001	0.410	6.248	0.434	37.219	6.565
J	6.493	0.578	7.675	0.739	39.350	6.196
K	5.732	0.818	6.981	0.927	38.299	8.922
M	5.402	0.592	6.566	0.741	34.733	2.571
N	5.528	0.336	6.681	0.337	33.543	2.123
O	5.698	0.304	6.780	0.392	36.392	6.736
1	0.797	0.440	1.081	0.555	10.221	3.512
2	0.641	0.555	0.803	0.663	5.016	3.121

Table 7
Average values of the roughness parameters Rz. Rp and Rv, for all samples.

| Sample	*Rz*		*Rp*		*Rv*	
	Average [μm]	Std dev [μm]	Average [μm]	Std dev [μm]	Average [μm]	Std dev [μm]
D	28.342	1.344	14.169	1.182	14.173	1.084
E	23.059	2.641	12.102	2.028	10.957	1.122
G	23.782	2.995	11.934	1.398	11.848	1.732
H	27.376	3.224	13.721	1.734	13.655	1.667
I	25.109	0.955	13.487	1.597	11.622	1.219
J	28.315	2.943	13.913	1.841	14.402	2.064
K	27.486	2.284	14.080	2.138	13.406	1.775
M	25.519	2.351	12.796	1.039	12.723	1.914
N	25.684	1.336	12.839	1.193	12.845	0.994
O	24.942	2.225	12.627	1.562	12.315	1.357
1	5.344	2.273	2.026	0.686	3.309	1.586
2	3.683	2.732	1.500	1.067	2.183	1.681
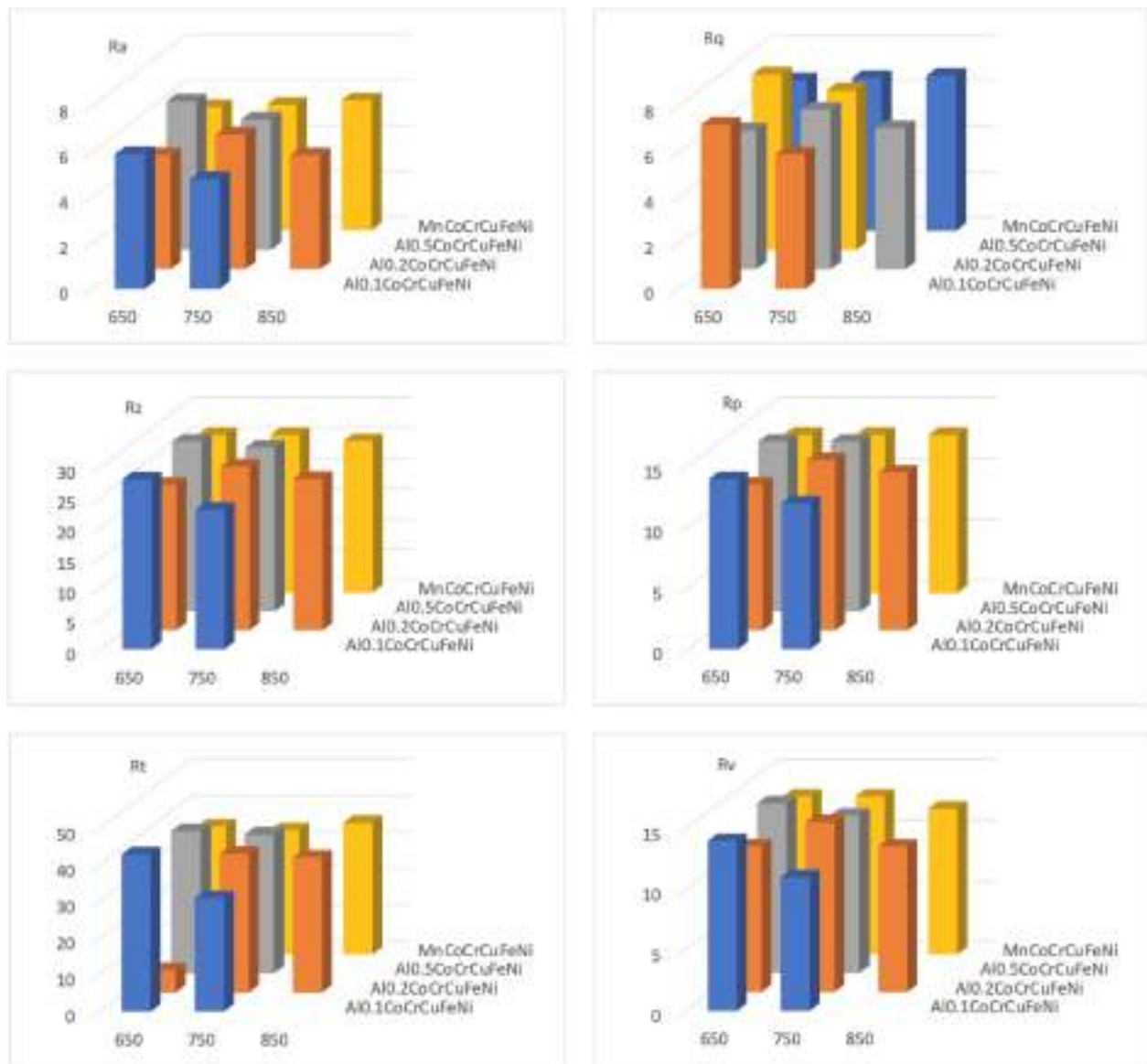
Fig. 7. Roughness parameters vs deposition temperature.

Table 8
Coating volume from profile measurements.

Specimen Id	Coating volume [mm^3]
D	1863
E	4069
G	3453
H	3549
I	3375
J	3584
K	3753
M	2251
N	3057
O	3589

Fig. 8. Coating volume from profile measurements.

The parameters of *Ra*, *Rq*, and *Rv* are maximum for sample I, while the parameters *Rt, Rz* and *Rp* are maximum for sample O. Based on the experimental data obtained, it cannot be concluded that the chemical composition of the high entropy alloy influences the roughness of the coating.
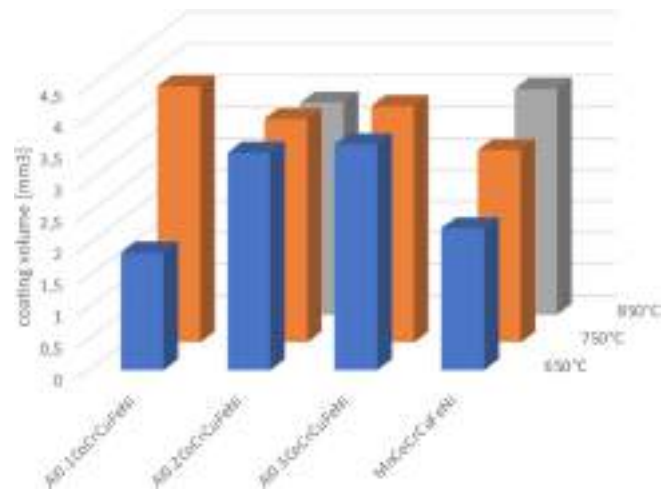
Table 9
Vickers microhardness measurements for samples D and E.

			Interface	Substrate	Coating
Al$_{0.1}$CoCrCuFeNi	D (650 °C)	Average	117,35	106,39	226,60
		Std dev	5,92	0,97	3,05
	E (750 °C)	Average	112,10	84,01	221,52
		Std dev	3,59	4,10	7,41
Al$_{0.2}$CoCrCuFeNi	G (650 °C)	Average	119,48	75,82	229,38
		Std dev	15,17	3,62	12,39
	H (750 °C)	Average	132,47	73,90	239,47
		Std dev	8,82	1,41	10,28
	I (850 °C)	Average	149,77	112,62	248,90
		Std dev	10,93	10,70	5,51
Al$_{0.5}$CoCrCuFeNi	J (650 °C)	Average	170,03	115,57	318,69
		Std dev	14,83	4,96	30,90
	K (750 °C)	Average	135,82	80,60	318,08
		Std dev	10,59	8,19	7,59
MnCoCrCuFeNi	M (650 °C)	Average	150,23	84,26	268,47
		Std dev	7,19	2,22	10,81
	N (750 °C)	Average	177,36	103,60	314,49
		Std dev	6,65	3,38	3,19
	O (850 °C)	Average	167,96	78,26	239,82
		Std dev	14,26	4,08	2,31
Mg Substrate	M1	Average		89,50	
		Std dev		2,40	
	M2	Average		76,12	
		Std dev		3,72	

3.2.2. Profile measurements

Results of coating volumes from profile measurements are reported in Table 8 and Fig. 8.

It results that the deposited volume increases with temperature only for Al$_{0.1}$ and Mg-based HEA, while for the other Al-based HEA no noticeable influences can be observed.

3.3. Microhardness test

On the lateral surface of the samples, after careful polishing, indentations were made at the interface between substrate and coating, on the coating at a distance of 100 μm from the interface, and on the substrate at a distance of 100 μm from the interface. A mean value was calculated for each position based on three measurements. An ANOVA analysis was performed to investigate the influence of deposition temperature and chemical composition on the microhardness parameter.

The microhardness values are shown in Table 9.

According to Table 9, the microhardness of a coating depends significantly on its chemical composition. As the percentage of aluminum present increases in the samples (D-K) with chemical composition AlxCoCrCuFeNi, an increasing trend with microhardness is evident. Samples of Al0.1CoCrCuFeNi composition (D-E) exhibit the lowest microhardness, while those of Al0.5CoCrCuFeNi composition (J-K) exhibit the maximum microhardness. Microhardness values were measured using the same parameters and procedures for samples 1 and 2 of magnesium substrates. The microhardness profiles obtained experimentally for various coating samples are presented in Figs. 9–12. The distance from the interface takes on negative values in the substrate area, while it takes on positive values in the coating area. According to the plots, the hardness of the coating is significantly higher than that of the substrate, and the hardness measured at the interface is intermediate between the two values. This result is due to the "hammering" effect, i.e. the progressive hardening of the material passing from the substrate to the coating due to the plastic deformation caused by the very high-speed impact of the alloy powders.

3.4. ANOVA results

In Fig. 13 the contour plots and surface plots for roughness and microhardness ANOVA study are reported.

An increase in the hardness of the coating was found as the atomic percentage of aluminum in the chemical composition increased for the groups belonging to the AlxCoCrCuFeNi system, in agreement with what was stated by the studies in the literature. The hardness of the MnCoCrCuFeNi composition coatings was found to be intermediate between those of the Al0.2CoCrCuFeNi and Al0.5CoCrCuFeNi groups; it also showed greater sensitivity to the temperature variation of the deposition process. Also in this case, it was not possible to identify a tendency for hardness to increase or decrease as the Cold Spray temperature increased, common to all groups of samples of similar
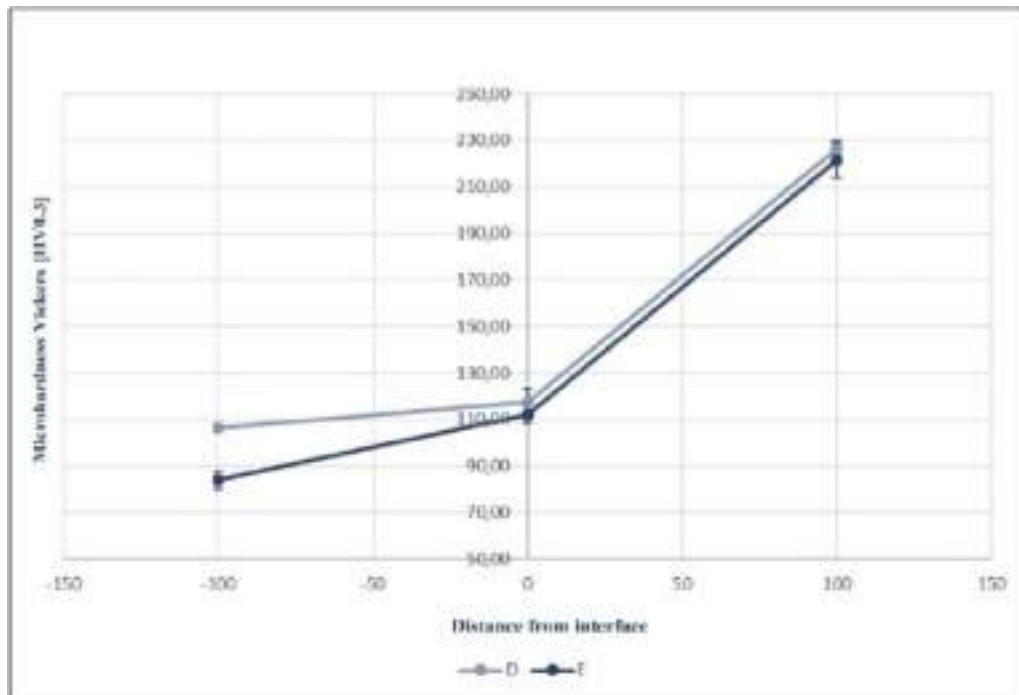

Fig. 9. Microhardness profiles for samples D and E vs distance from the interface.
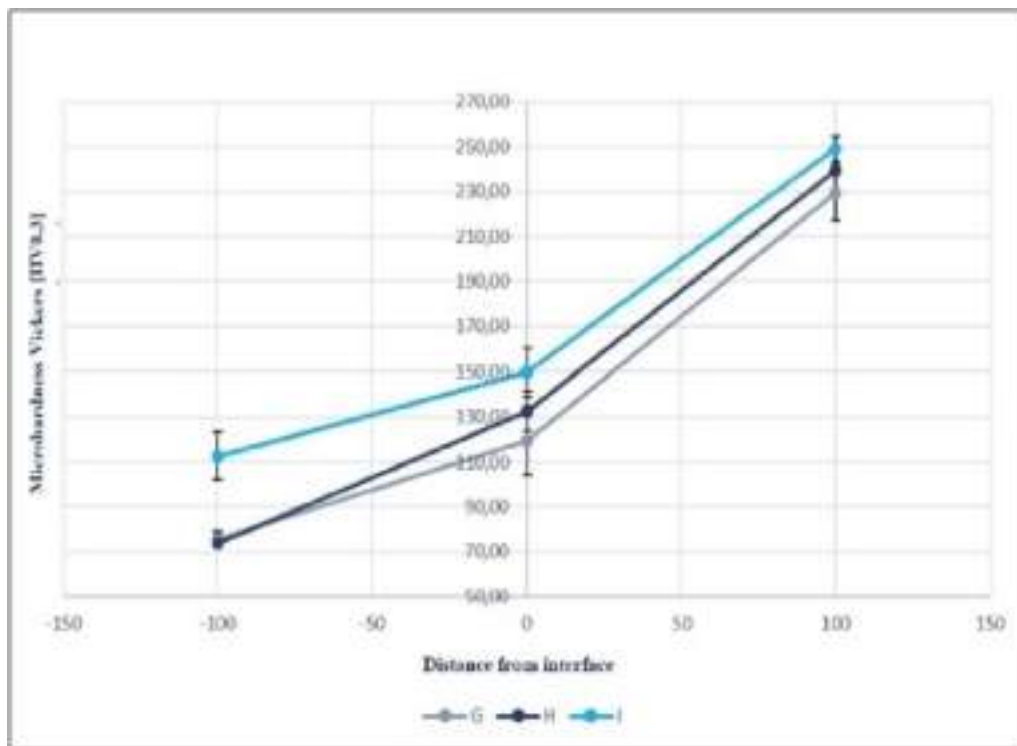
Fig. 10. Microhardness profiles for samples G, H, and I vs distance from the interface.
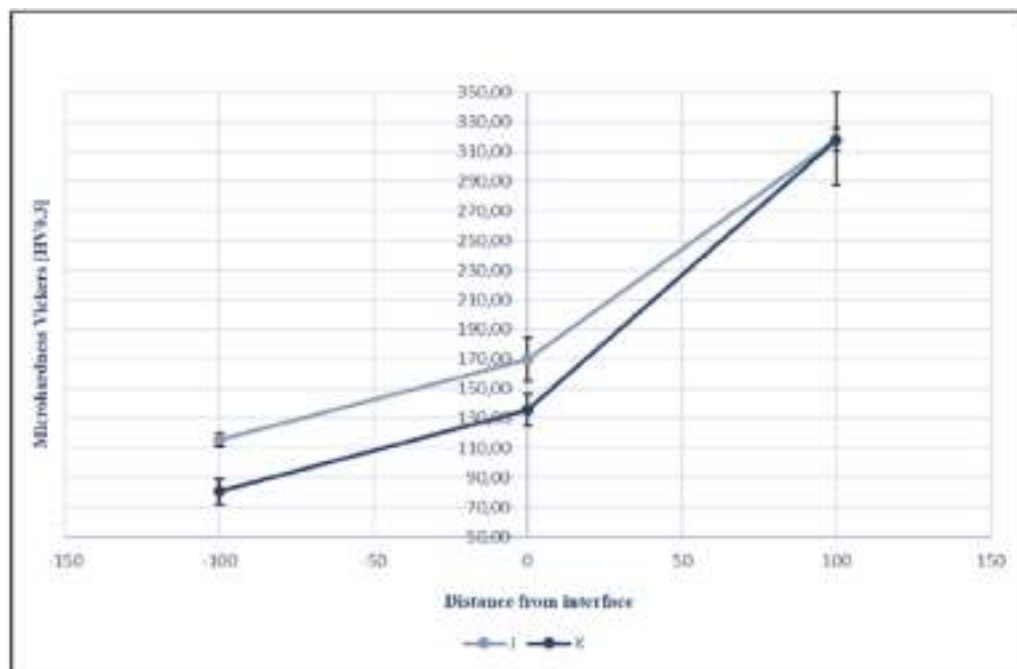

Fig. 11. Profiles of microhardness vs distance from the interface for samples J and K.

composition. The samples of composition Al0.2CoCrCuFeNi showed an increase in hardness as the deposition temperature increased, while those of composition Al0.1CoCrCuFeNi showed a decrease. For the samples of composition Al0.5CoCrCuFeNi the hardness was approximately constant, while for those of composition MnCoCrCuFeNi a non-monotonic trend was found as the Cold Spray temperature increased, with the maximum value for the N sample, deposited at the intermediate level temperature (equal to 750 °C).

Statistical analysis of variance (ANOVA), applied using the experimental data, demonstrated that:

1) The average roughness of the surface of the coatings of the samples of the AlxCoCrCuFeNi composition group, in as-sprayed conditions, is influenced in a statistically significant way both by the atomic percentage of aluminum present and by the temperature of the deposition process, but not by the interaction of the two factors. The
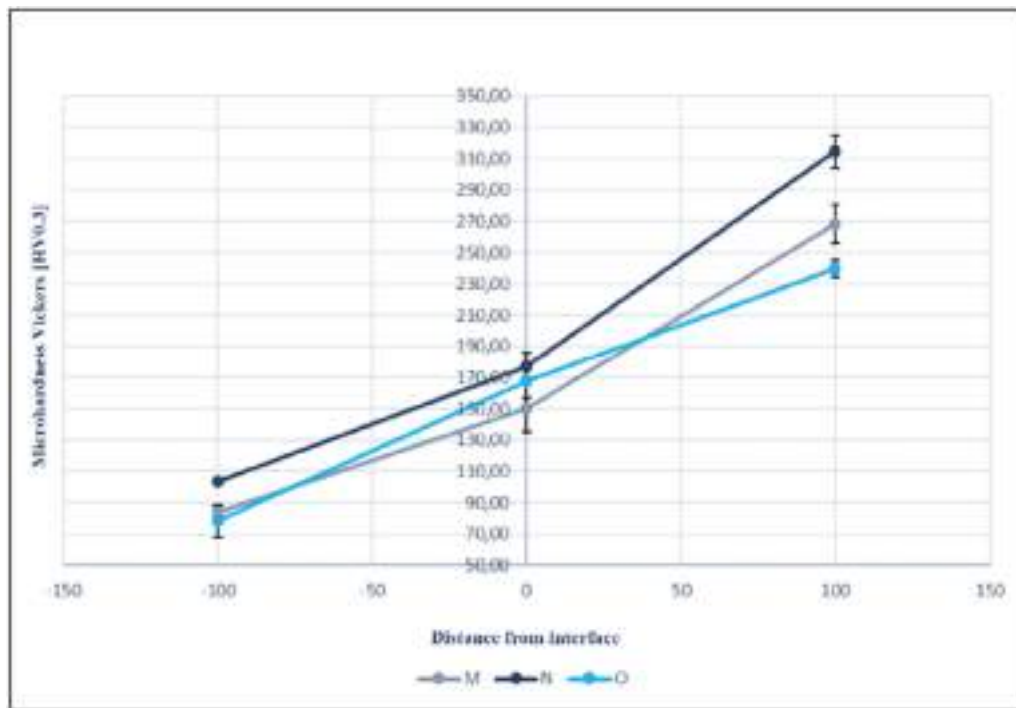
Fig. 12. Profiles of microhardness vs distance from the interface for samples M, N, and O.

average roughness decreased as the Cold Spray temperature increased and increased as the percentage of aluminum increased.

2) The hardness of the coatings of the samples of the AlxCoCrCuFeNi composition group, at a distance of 100 μm from the interface, is influenced in a statistically significant way by the atomic percentage of aluminum present, but not by the temperature of the Cold Spray deposition process. In particular, the hardness, as expected, increased as the percentage of aluminum present increased. The interaction between the two factors considered did not demonstrate a significant influence.

4. Conclusions

Mechanical Alloying and Cold Spray processed $Al_{0.1-0.5}$(Mn) CoCuCrFeNi HEA coating surface, deposited on Mg substrate, using N_2 as the process gas with three different gas temperatures, was characterized in microstructure, roughness, and hardness properties.

Based on the results obtained in this research, the following conclusions can be drawn.

Mechanical Alloying caused plastic deformation and fracture of A2 and B2 harder particles. Relatively soft and ductile A1 phase and Cu-rich region particles were coarser and globular in shape. Some separate Cu-rich regions were also observed apart from A1 particles. Mn-HEA powder showed a different trend with finer particle sizes due to the more brittle nature of the powder and acicular shape. SEM surface morphology of the $Al_{0.1}$CoCuCrFeNi powder milled for 5.5 h shows fine to moderate size A2/B2 particles. Moreover, coarser particles for both A1 and Cu-reach regions and very fine surface Cr_2O_3 particles were observed with light microscopy (LM) and powder size distribution (PSD) study. It was also observed that, during MA, there was a loose structure with lots of gaps, cracks, plastic deformation signs, and small particles adhering to the particle surface. Particle surfaces were also rough due to heavy plastic deformation, cold welding, and fracture mechanisms induced by MA processing. The elemental powder size chosen during MA was influenced by metallic elements' hardness and ductility as, in the $Al_{0.1}$CoCuCrFeNi HEA system, they exhibit high plasticity and go through plastic deformation, cold welding, and fracture processes. All the coatings showed good bonding with their substrates, free of pores and cracks, mechanical interlocking was observed along the coating-substrate interface and some particles penetrated the substrate and were tightly bound by the material, resulting in the coating's high adhesion strength. The coatings show a dense microstructure with only a few pores. Porosity results of specimens were in the range 1.5–3.2 %. Specimens in $Al_{0.1}$CoCrCuFeNi show a decrease in all roughness parameters with increasing deposition temperature. For other specimens, a monotonic relationship between the roughness parameters and the temperature of the deposition process cannot be stated. Based on the experimental data obtained, it cannot be concluded that the chemical composition of the high entropy alloy influences the roughness of the coating. The deposited volume increases with temperature only for $Al_{0.1}$ and Mg-based HEA, while for the other Al-based HEA no noticeable influences can be observed. The microhardness of a coating depends significantly on its chemical composition. As the percentage of aluminum increases in the samples an increasing trend with microhardness is evident. The hardness of the coating is significantly higher than that of the substrate, and the hardness measured at the interface is intermediate between the two values.

Results are confirmed by ANOVA analysis.

CRediT authorship contribution statement

Raffaella Sesana: Data curation, Supervision, Writing – review & editing. **Nazanin Sheibanian:** Data curation, Formal analysis, Methodology, Writing – original draft. **Luca Corsaro:** Data curation, Formal analysis, Methodology, Writing – original draft. **Sedat Özbilen:** Conceptualization, Data curation, Formal analysis, Funding acquisition. **Rocco Lupoi:** Funding acquisition. **Francesco Artusio:** Data curation, Methodology.

Declaration of competing interest

The authors declare that they have no known competing financial interests or personal relationships that could have appeared to influence the work reported in this paper.
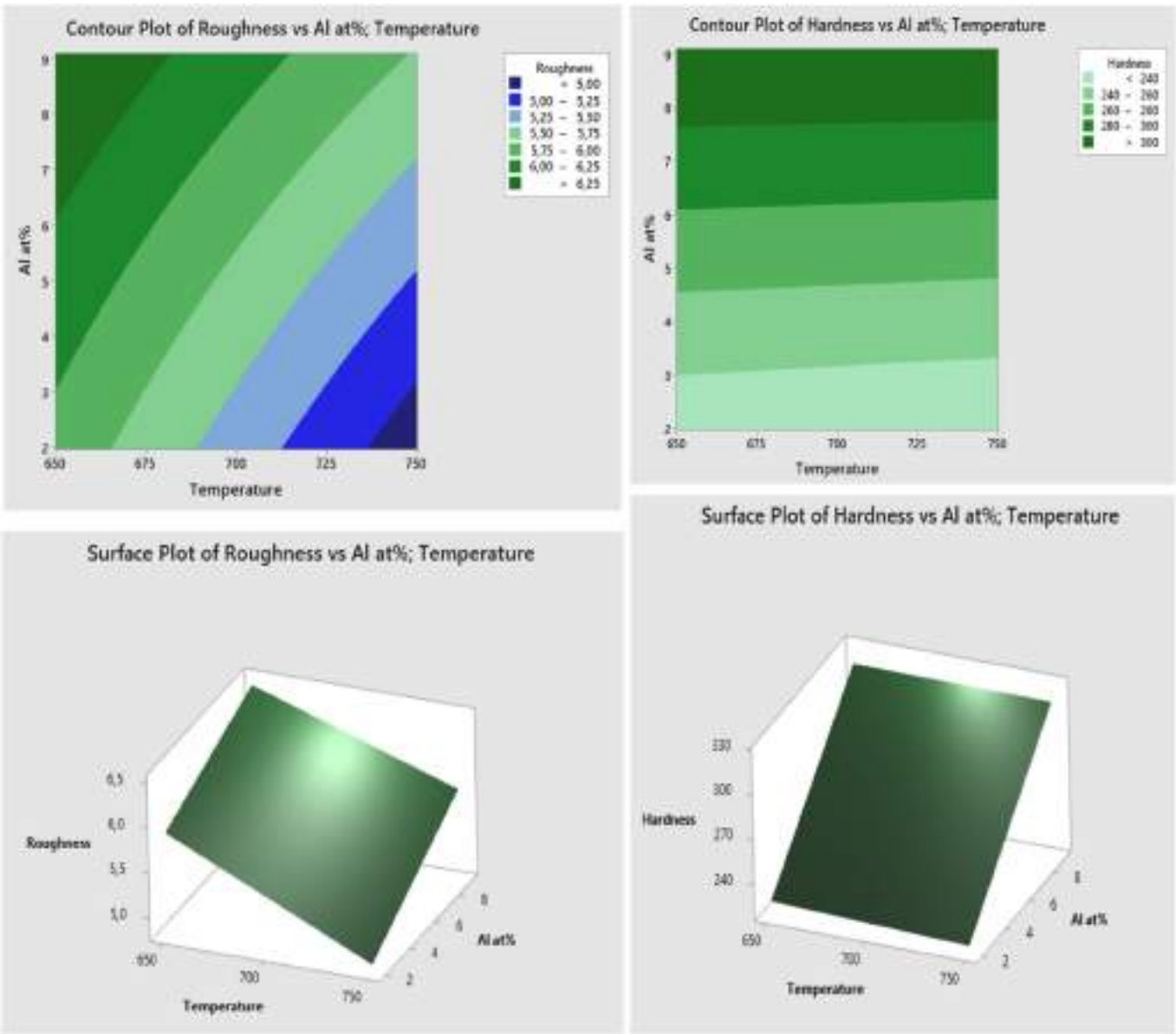
Fig. 13. Contour plot (above) e surface plot (below) of roughness (left) and Vickers microhardness (right) ANOVA models.

Data availability

Data will be made available on request.

Acknowledgement

Appendix. hardness measurements (Vickers)

Specimen		Interface	Substrate	Coating
D – 650°	Meas 1	120,65	107,24	230,1
	Meas 2	120,89	105,34	224,51
	Meas 3	115,23	104,30	221,12
	Meas 4	117,41	106,70	221,19
	Meas 5	110,52	106,60	225,18
	Mean	116,94	106,04	224,42

(*continued on next page*)

(*continued*)

Specimen		Interface	Substrate	Coating
	Std dev	4,29	1,19	3,68
Specimen		interface	substrate	coating
E – 750°	Meas 1	109,55	88,46	218,59
	Meas 2	110,54	83,18	229,95
	Meas 3	112,14	87,54	220,68
	Meas 4	111,34	82,43	212,44
	Meas 5	116,21	80,39	216,03
	Mean	111,96	84,40	219,54
	Std dev	2,56	3,46	6,58
G – 650°	Meas 1	119,43	79,37	224,78
	Meas 2	134,67	75,94	243,41
	Meas 3	124,87	76,45	234,56
	Meas 4	115,93	77,23	228,45
	Meas 5	104,33	72,14	219,94
	Mean	119,85	76,23	230,23
	Std dev	11,19	2,63	9,10
H – 750°	Meas 1	141,96	74,20	250,47
	Meas 2	130,92	72,36	230,11
	Meas 3	136,60	70,51	245,2
	Meas 4	129,43	73,94	240,07
	Meas 5	124,52	75,13	237,84
	Mean	132,69	73,23	240,74
	Std dev	6,74	1,82	7,69
I – 850°	Meas 1	155,20	123,78	254,19
	Meas 2	137,18	102,45	243,2
	Meas 3	152,50	116,52	250,89
	Meas 4	145,98	112,64	251,31
	Meas 5	156,92	111,62	249,31
	Mean	149,56	113,40	249,78
	Std dev	8,07	7,76	4,08
J – 650°	Meas 1	152,90	116,37	344,76
	Meas 2	178,68	110,26	275,28
	Meas 3	161,99	112,45	320,98
	Meas 4	170,45	115,90	300,87
	Meas 5	178,50	120,08	336,02
	Mean	168,50	115,01	315,58
	Std dev	11,10	3,79	28,01
K – 750°	Meas 1	128,53	89,09	324,12
	Meas 2	130,96	79,97	320,57
	Meas 3	135,88	80,56	315,67
	Meas 4	132,49	78,97	322,45
	Meas 5	147,97	72,75	309,56
	Mean	135,17	80,27	318,47
	Std dev	7,64	5,84	5,90
M – 650°	Meas 1	155,50	82,70	259,91
	Meas 2	153,14	86,80	280,61
	Meas 3	148,53	85,60	278,91
	Meas 4	150,96	86,78	262,56
	Meas 5	142,04	83,27	264,88
	Mean	150,03	85,03	269,37
	Std dev	5,16	1,94	9,66
N – 750°	Meas 1	178,59	99,70	314,3
	Meas 2	183,31	105,76	317,77
	Meas 3	175,60	103,47	318,92
	Meas 4	172,42	100,96	315,64
	Meas 5	170,18	105,33	311,39
	Mean	176,02	103,04	315,60
	Std dev	5,17	2,66	2,96
O – 850°	Meas 1	152,63	73,62	240,36
	Meas 2	170,42	81,31	237,29
	Meas 3	164,78	79,23	241,46
	Meas 4	175,62	75,44	238,88
	Meas 5	180,83	79,84	241,82
	Mean	168,86	77,89	239,96
	Std dev	10,86	3,22	1,88
Specimen				
Mg substrate M1	Meas 1			91,40
	Meas 2			86,80
	Meas 3			89,21
	Meas 4			88,48
	Meas 5			90,30
	Mean			89,24
	Std dev			1,76
Mg substrate M2	Meas 1			79,29
	Meas 2			77,04
	Meas 3			74,82

(*continued*)

Meas 4	78,13
Meas 5	72,03
Mean	76,26
Std dev	2,88

References

[1] B.S. Murty, S. Ranganathan, J.W. Yeh, High-Entropy Alloys, Butterworth-Heinemann, Burlington, 2014. Web.

[2] Ming-Hung Tsai, Jien-Wei Yeh, High-entropy alloys: a critical review, Mater. Res. Lett. 2 (3) (2014) 107–123. Web.

[3] Shuo Yin, Wenya Li, Bo Song, Xingchen Yan, Min Kuang, Yaxin Xu, Kui Wen, Rocco Lupoi, Deposition of FeCoNiCrMn high entropy alloy (HEA) coating via cold spraying, J. Mater. Sci. Technol. 6 (2019) 1003–1007. Web.

[4] Roghayeh Nikbakht, Mohammad Saadati, Taek-Soo Kim, Mohammad Jahazi, Hyoung Seop Kim, Jodoin Bertrand, Cold spray deposition characteristic and bonding of CrMnCoFeNi high entropy alloy, Surf. Coating. Technol. (2021) 127748. Web.

[5] Jian Wu, Yujie Chen, Heguo Zhu, A review on the tribological performances of high-entropy alloys, Adv. Eng. Mater. 8 (2022) 2101548. N/a. Web.

[6] Dawei Luo, Qing Zhou, Zhuobin Huang, Yulong Li, Yulin Liu, Qikang Li, Yixuan He, Haifeng Wang, Tribological behavior of high entropy alloy coatings: a review, Coatings 12 (10) (2022) 1428. Web.

[7] Gifty, Oppong Boakye, et al., Microstructural properties and wear resistance of Fe-Cr-Co-Ni-Mo-based high entropy alloy coatings deposited with different coating techniques, Appl. Sci. 12 (6) (2022) 3156. ProQuest.Web. 14 Nov. 2022.

[8] Jiayi Xia, Dongqun Xin, Xizhang Chen, Heyang Xin, Investigation of the microstructure and friction mechanism of novel CoCrCu0.2FeMox high-entropy alloy coating using plasma arc cladding, Met. Corros. (2022).

[9] D.B. Miracle, O.N. Senkov, A critical review of high entropy alloys and related concepts, Acta Mater. 122 (2017) 448–511. Web.

[10] Yong Zhang, Ting Ting Zuo, Zhi Tang, Michael C. Gao, Karin A. Dahmen, Peter K. Liaw, Zhao Ping Lu, Microstructures and properties of high-entropy alloys, Prog. Mater. Sci. 61 (2014) 1–93. Web.

[11] M.A. Hemphill, T. Yuan, G.Y. Wang, J.W. Yeh, C.W. Tsai, A. Chuang, P.K. Liaw, Fatigue behavior of Al0.5CoCrCuFeNi high entropy alloys, Acta Mater. 60 (2012) 5723–5734.

[12] C.J. Tong, M.R. Chen, J.W. Yeh, et al., Mechanical performance of the AlxCoCrCuFeNi high-entropy alloy system with multiprincipal elements, Metall. Mater. Trans. A 36 (2005) 1263–1271.

[13] Yongming Zou, Zhaoguo Qiu, Chunjie Huang, Dechang Zeng, Rocco Lupoi, Nannan Zhang, Shuo Yin, Microstructure and tribological properties of Al2O3 reinforced FeCoNiCrMn high entropy alloy composite coatings by cold spray, Surf. Coat. Technol. 434 (2022) 128205. Web.

[14] Jien-Min Wu, Su-Jien Lin, Jien-Wei Yeh, Swe-Kai Chen, Yuan-Sheng Huang, Hung-Cheng Chen, Adhesive wear behavior of AlxCoCrCuFeNi high-entropy alloys as a function of aluminum content, Wear 261 (5–6) (2006), 513-19. Web.

[15] Jin-Kun Xiao, Hong Tan, Yu-Qing Wu, Juan Chen, Chao Zhang, Microstructure and wear behavior of FeCoNiCrMn high entropy alloy coating deposited by plasma spraying, Surf. Coat. Technol. 385 (2020) 125430. Web.

[16] Baosen Zhang, Yaqiu Yu, Shuaishuai Zhu, Zhijia Zhang, Xuewei Tao, Zhangzhong Wang, Bin Lu, Microstructure and wear properties of TiN–Al2O3–Cr2B multiphase ceramics in-situ reinforced CoCrFeMnNi high-entropy alloy coating, Mater. Chem. Phys. 276 (2022) 125352. Web.

[17] S.S. Liu, M. Zhang, G.L. Zhao, X.H. Wang, J.F. Wang, Microstructure and properties of ceramic particle reinforced FeCoNiCrMnTi high entropy alloy laser cladding coating, Intermetallics 140 (2022) 107402. Web.

[18] Shuaishuai Zhu, Yaqiu Yu, Baosen Zhang, Zhijia Zhang, Xiao Yan, Zhangzhong Wang, Microstructure and wear behaviour of in-situ TiN-Al2O3 reinforced CoCrFeNiMn high-entropy alloys composite coatings fabricated by plasma cladding, Mater. Lett. 272 (2020) 127870. Web.

[21] S. Ozbilen, R. Lupoi, Al0. 5 HEA Protective Coatings on Mg Based Parts by Mechanical Alloying, Cold Spraying and Argon Annealing, TSA, Technology Transfer Office, TCD, Dublin, Ireland, February 2023.

[22] S. Yin, R. Lupoi, C. Chen, Property enhancement of cold sprayed Al-diamond MMC coating by using core-shelled diamond reinforcements, Proc. Int. Therm. Spray Conf. 2019 (2019) 469–475.

[23] R. Lupoi, M. Meyer, W.W. Wits, S. Yin, The role of particles flow characteristics in the performance of cold spray nozzles, CIRP Ann. 69 (2020) 189–192.

[24] S. Ozbilen, J.F.B. Vasquez, W. Abbott, S. Yin, M. Morris, R. Lupoi, Mechanical milling, characterisation, and phase prediction of Al$_{0.1-0.5}$(Mn)CoCrCuFeNi HEA powder feedstock for cold spray deposition processing, under revision, J. Alloys Compd. (May 2023), https://doi.org/10.1016/j.jallcom.2023.170854.

[25] Ozbilen, R. Sesana L. Corsaro, N. Sheibanian, V. Ott, J. F. B. Vasquez, M. Stueber S. Ulrich M. Morris, R. Lupoi, Structure and properties of Al$_{0.1-0.5}$(Mn)CoCrCuFeNi HEA coatings on Mg fabricated by combined mechanical alloying and cold spraying at different CS nitrogen gas temperature, J. Mater. Sci. Technol. Chin. Soc., under revision June 2023..

Further reading

[19] Yiku Xu, Geng Wang, Song Qi, Xinyu Lu, Zhiyuan Li, Qinyang Zhao, Yongnan Chen, Microstructure, mechanical properties, and corrosion resistance of SiC reinforced AlxCoCrFeNiTi1-x high-entropy alloy coatings prepared by laser cladding, Surf. Coat. Technol. 437 (2022) 128349. Web.

[20] Da Sun, Lisong Zhu, Yangchuan Cai, Yanan Yan, Fuyu Ge, Mengdie Shan, Yinbao Tian, Jian Han, Zhengyi Jiang, Tribology comparison of laser-cladded CrMnFeCoNi coatings reinforced by three types of ceramic (TiC/NbC/B4C), Surf. Coat. Technol. 450 (2022). Surface & Coatings Technology, 2022, Vol.450. Web.